SUPPLEMENTAL MATERIAL

Cerboni et al., https://doi.org/10.1084/jem.20161674

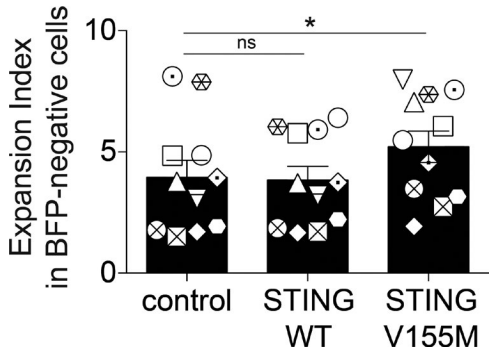

Figure S1. **Proliferation of BFP–negative T cells.** Expansion index in BFP-negative and proliferating cells as in Fig. 1 D. $n = 11$. Data are mean ± SEM. One-way ANOVA with Tukey's correction was used. *, $P < 0.05$.

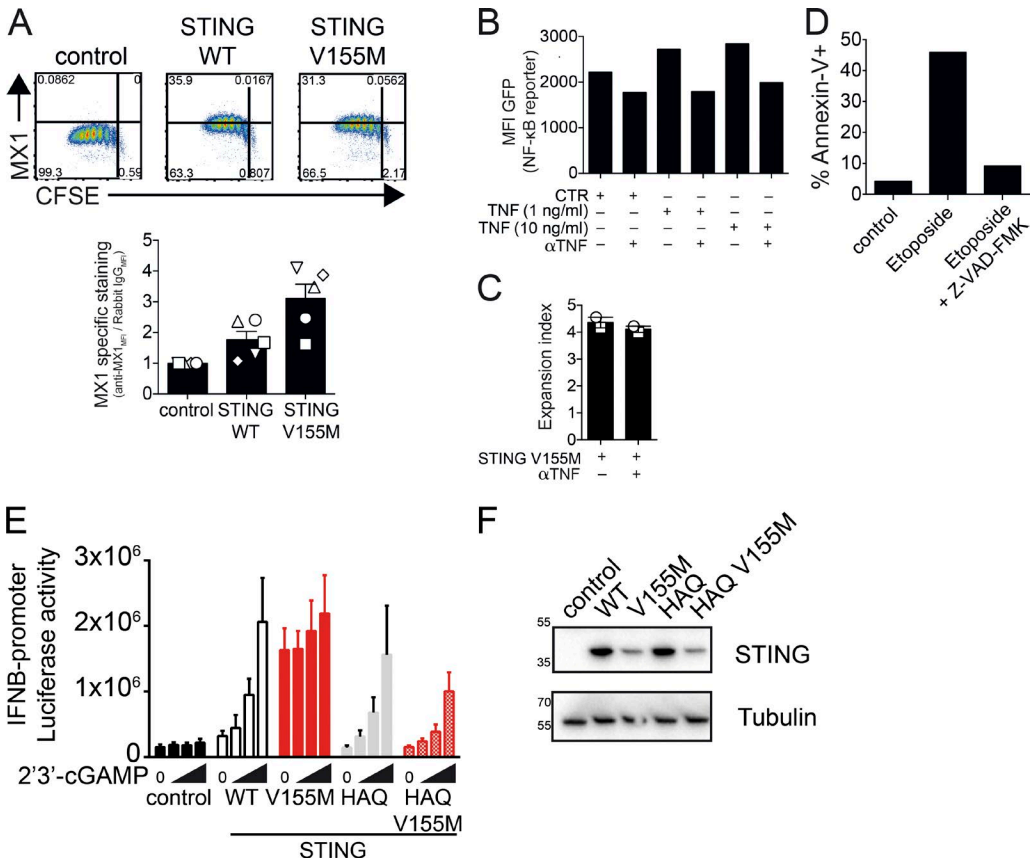

Figure S2. **Controls for STING V155M activation.** (A) Intracellular MX1 expression and proliferation profile (CFSE) in naive CD4$^+$ T cells transduced with control, STING WT, or STING V155M BFP lentivectors. $n = 5$ donors. Data are mean ± SEM. MFI, mean fluorescence intensity. (B) GFP expression in naive CD4$^+$ T cells transduced with a lentivector coding for GFP under the control of an NF-κB reporter promoter, after treatment with recombinant TNF or neutralizing anti-TNF antibody. Data are representative of $n = 2$ donors. CTR, control. (C) Expansion index as in Fig. 2 D. $n = 2$. Data are mean ± SEM. (D) Annexin V staining in naive CD4$^+$ T cells as in Fig. 2 E, after treatment with 25 µM etoposide or etoposide with 50 µM Z-VAD-FMK. Data are representative of $n = 2$ donors. (E) Luciferase activity in 293FT cells cotransfected with empty vector, STING variants, and a Luciferase-coding plasmid under control of the human IFNB promoter, stimulated with increasing amounts of synthetic 2′3′-cGAMP (top dose, 4 µg/ml; threefold dilutions). $n = 3$ independent experiments. Mean and SEM are plotted. (F) Immunoblot of STING and actin expression in 293FT transfected cells as in E. Molecular mass is shown in kilodaltons.

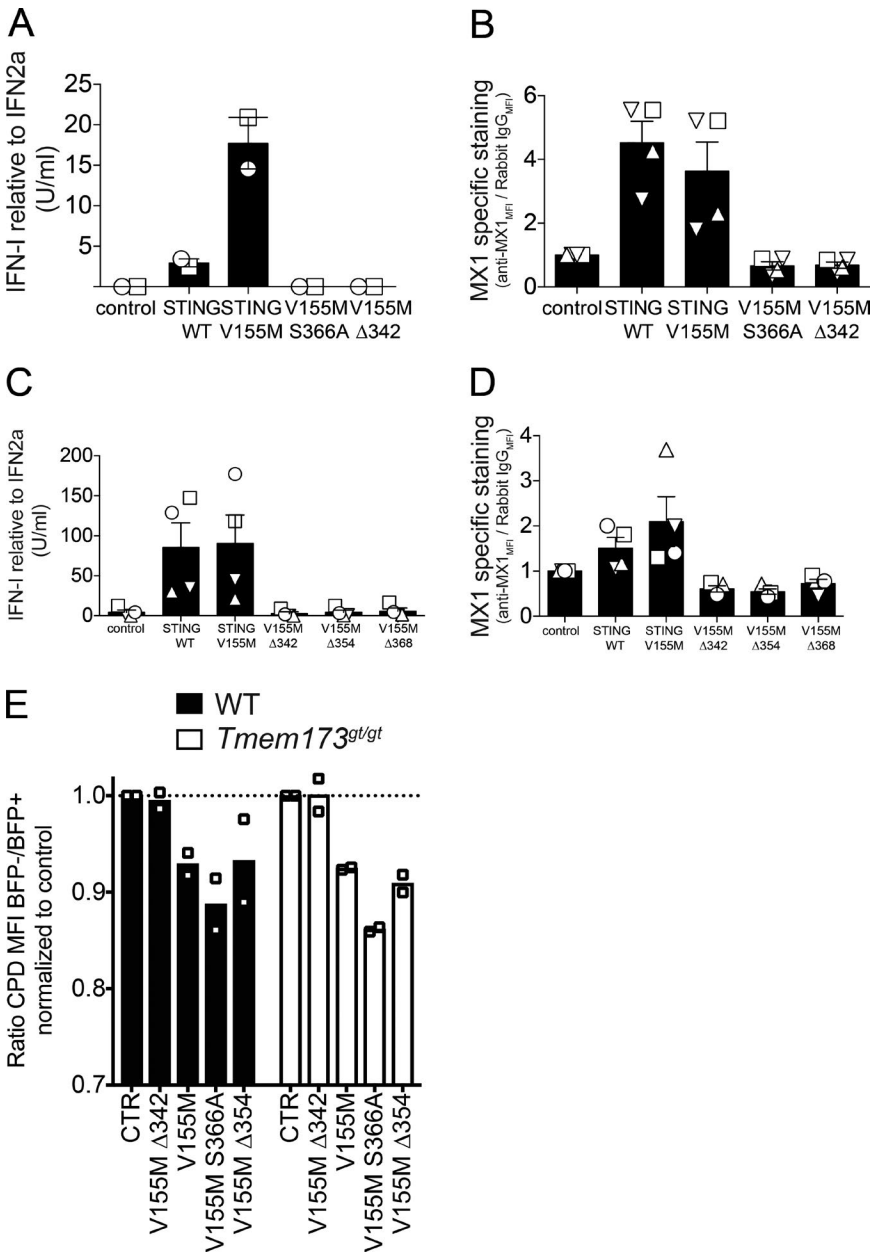

Figure S3. **Activities mediated by STING miniCTT in human and mouse T cells.** (A) Type I IFN activity in supernatants of naive CD4+ T cells 4 d after transduction with control, STING WT, V155M, V155M S366A, or V155M Δ342 BFP lentivectors. *n* = 2 independent donors. (B) Specific intracellular MX1 staining in naive CD4+ T cells 4 d after transduction with control, STING WT, V155M, V155M S366A, or V155M Δ342 BFP lentivectors. *n* = 2. (C) Type I IFN activity in supernatants of naive CD4+ T cells 4 d after transduction with control, STING WT, V155M, V155M Δ342, V155M Δ354, or V155M Δ368 BFP lentivectors. *n* = 2 independent donors. (D) Intracellular staining of MX1 in naive CD4+ T cells 4 d after transduction with control, STING WT, V155M, V155M Δ342, V155M Δ354, or V155M Δ368 BFP lentivectors. *n* = 2 independent donors. (E) Ratio of proliferation between transduced (BFP positive) and untransduced (BFP negative) mouse CD4+ T cells after transduction with the indicated lentivectors. *n* = 2 independent mice. Data are mean ± SEM. CPD, cell proliferation profile; CTR, control; MFI, mean fluorescence intensity.

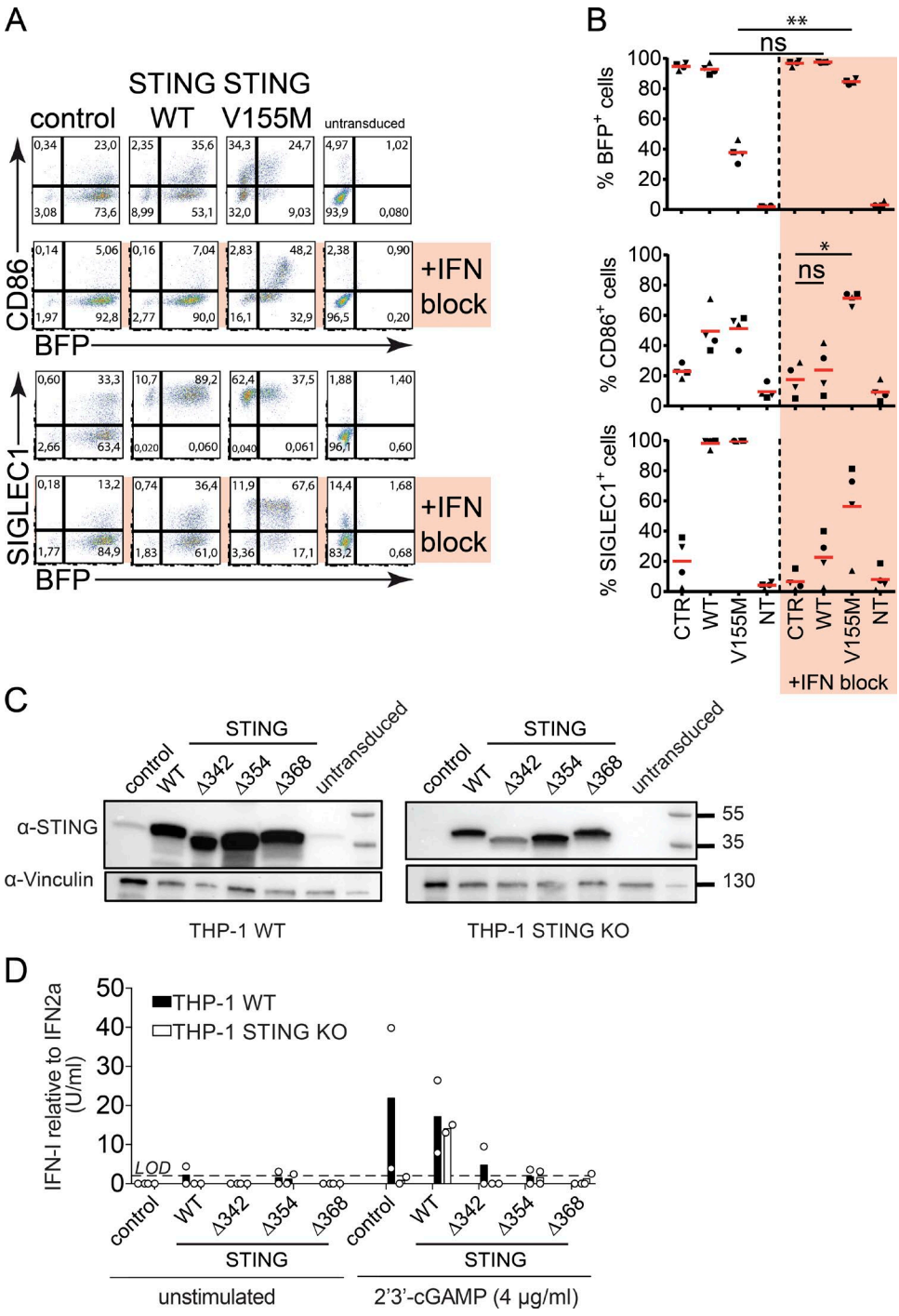

Figure S4. **Activities mediated by STING miniCTT in human DCs and STING KO THP-1 cells.** (A) Neutralization of type I IFN enables lentiviral transduction of DCs with STING V155M, revealing the ability of STING V155M to activate DCs. BFP, CD86, and SIGLEC1 expression in DCs 4 d after transduction with control, STING WT, or STING V155M BFP lentivectors and neutralization of type I IFN. (B) BFP, CD86, and SIGLEC1 expression as in A. $n = 4$ independent donors combined from two experiments. One-way ANOVA with Tukey's posthoc test was used. *, $P < 0.05$; **, $P < 0.01$. CTR, control; NT, not transduced. (C) Immunoblot of STING and vinculin in THP-1 WT and THP-1 STING KO cells transduced with the indicated BFP lentivectors. Molecular mass is shown in kilodaltons. (D) Type I IFN activity in supernatants of THP-1 WT and THP-1 STING KO cells transduced with the indicated BFP lentivectors, after no stimulation or stimulation with 2′3′-cGAMP–Lipofectamine. $n = 2$ independent experiments. LOD, limit of detection.

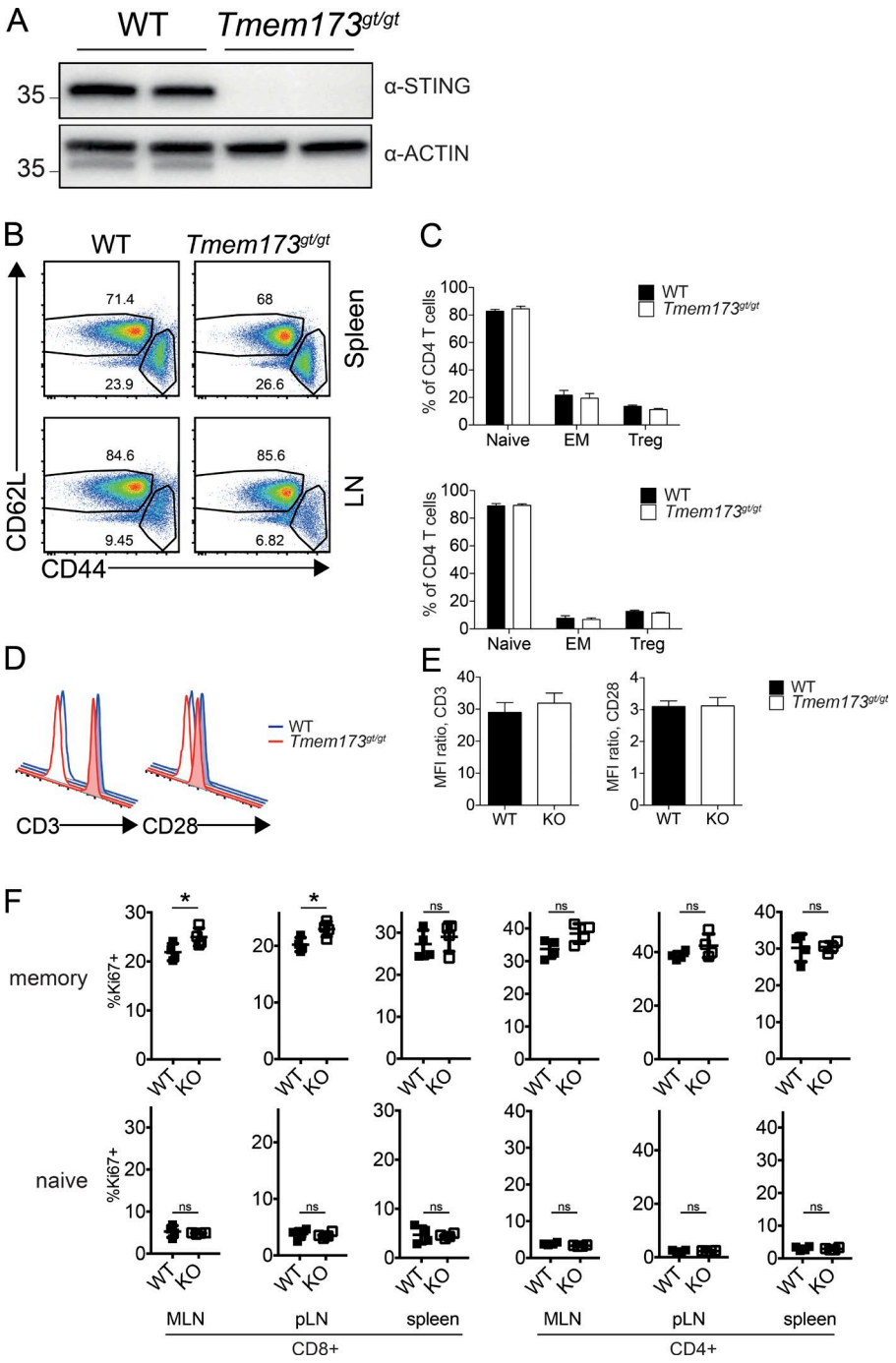

Figure S5. **Phenotypes of T cells from *Tmem173*-deficient mice.** (A) Immunoblot of STING and actin expression in CD8$^+$ T cells pooled from spleen and lymph nodes of WT and *Tmem173*$^{gt/gt}$ mice. $n = 2$. Molecular mass is shown in kilodaltons. (B) Representative dot plots of CD4$^+$ T cell subpopulations in spleens (top) or peripheral lymph nodes (bottom) of WT or *Tmem173*$^{gt/gt}$ mice. (C) Quantification of CD4$^+$ T cell subpopulations in spleens (top) or lymph node (bottom) of WT or *Tmem173*$^{gt/gt}$ mice. $n = 4$ mice from two independent experiments. Data are mean + SEM. EM, effector memory; Treg, regulatory T cell. (D) Representative histogram plots showing expression of CD3 and CD28 surface expression in naive CD4$^+$ T cells from WT or *Tmem173*$^{gt/gt}$ mice. Solid color filling indicates specific antibody, and white filling indicates isotype control staining. (E) Quantification of CD3 and CD28 expression on naive CD4$^+$ T cells from WT or *Tmem173*$^{gt/gt}$ mice. $n = 4$ mice from two independent experiments. Data are mean + SEM. MFI, mean fluorescence intensity. (F) Percentage of Ki67-expressing WT or STING-deficient naive and memory CD4$^+$ and CD8$^+$ T cells from lymphoid organs of CD3ε/WT or CD3ε/Tmem173$^{gt/gt}$ (KO) mixed bone marrow chimeras. $n = 4$ mice from two independent groups. Data are mean ± SEM. *, $P < 0.05$. Unpaired Student's *t* test on log-transformed data was used. mLN, mesenteric lymph node; pLN, peripheral lymph node.

Table S1. **Clinical immunophenotype of patients carrying an activating *TMEM173* mutation**

	Age group 1		Age group 2				Age group 3	
	P1	Expected values	P5	P7	P11	Expected values	P10	Expected values
TMEM173 mutation	V155M		V155M	V147M	N154S		V155M	
Age at analysis	2		11	8	7		14	
Absolute counts								
$CD3^+$	3,060	1,400–3,700	1,782	1,560	1,444	1,200–2,600	**558**	1,200–2,600
$CD4^+$	1,935	700–2,200	999	960	819	650–1,500	**270**	650–1,500
$CD8^+$	945	490–1,300	729	560	566	370–1,100	**270**	370–1,100
$CD19^+$	1,170	390–1,400	621	380	410	270–860	**1,206**	110–570
$CD16^+CD56^+$	225	130–720	270	**60**	**98**	100–480	**36**	70–480
Percentage								
T cells								
$CD3^+$%	68	56–75	66	**78**	74	60–76	**31**	56–84
$CD4^+$%	43	28–47	37	**48**	42	31–47	**15**	31–52
$CD8^+$%	21	16–30	27	28	29	18–35	**15**	18–35
$CD45RO^+CD4^+$%	**10**	14–27	**16**	**6**	**8**	30–42	**20**	30–42
$CD45RA^+CD4^+$%	**90**	73–86	**84**	**94**	**92**	58–70	**80**	58–70
$CD31^+CD45RA^+/CD4^+$%	**74**	57–65	**65**	51	**47**	43–55	55	43–55
$CCR7^+CD45RA^+/CD8^+$%	**88**	52–68	**86**	**80**	**82**	52–68	**94**	52–68
$CCR7^+CD45RA^-/CD8^+$%	**1**	3–4	**1**	4	3	3–4	4	3–4
$CCR7^-CD45RA^-/CD8^+$%	**3**	11–20	**5**	**7**	**3**	11–20	**1**	11–20
$CCR7^-CD45RA^+/CD8^+$%	**8**	16–28	**8**	**9**	**12**	16–28	**1**	16–28
$CD19^+$%	30	14–33	23	19	21	13–27	**67**	6–23
$CD27^+$/ $CD19^+$%	**1.8**	>10	ND	**4**	ND	14.7–25.8	**0.7**	12.6–25.2
$CD16^+CD56^+$%	5	4–17	10	3	5	4–17	**2**	3–22

Bold and underlining indicate values outside of the expected range. ND, not determined.